World Scientific
www.worldscientific.com

Glycerol effects on optical, weight and geometrical properties of skin tissue

Vadim D. Genin*,†, Elina A. Genina*,†,§, Valery V. Tuchin*,†,‡ and
Alexey N. Bashkatov*,†

*Saratov State University (National Research University)
83, Astrakhanskaya Str., Saratov 410012, Russia

†Tomsk State University (National Research University)
36, Lenina Av., Tomsk 634050, Russia

‡Institute of Precise Mechanics and Control of RAS
24, Rabochaya Str., Saratov 410028, Russia
§eagenina@yandex.ru

Complex study of glycerol effects on the skin tissue was performed. The change in optical, weight and geometrical parameters of the rat skin under the action of the glycerol solutions was studied *ex vivo*. Possible mechanisms of the skin optical clearing under the action of glycerol solutions of different concentrations were discussed. The results can be helpful for refinement of models developed to evaluate the effective diffusion coefficients of glycerol in tissues.

Keywords: Glycerol solutions; skin; optical clearing; collimated transmittance; dehydration.

1. Introduction

Interest in the use of optical clearing agents (OCAs) for improvement of optical methods for diagnostics and therapy of various diseases as well as differentiation of healthy and pathologically varied tissues constantly increases because they are safe and inexpensive.[1,2] Glycerol is one of the most popular biocompatible OCAs widely used for tissue optical cleaning (OC). Glycerol ($C_3H_8O_3$) is the simplest triol. It can be found in all natural fats and oils as fatty esters and is an important intermediate in the metabolism of living organisms. Glycerol is a viscous hygroscopic liquid with molecular weight (MW) 92.1 Da.[3] Penetration of glycerol and its aqueous solutions[4–14] were investigated for different health and pathological tissues. Partially, using glycerol as an OCA opens the way for the therapy of tissues hidden under bones, cartilages, tendons, etc.[15,16] Cicchi *et al.*[17] presented the first studies of two-photon in-depth enhancement under treatment with OCAs. Huang *et al.*[18] investigated the OC effect of glycerol on the porcine skin tissue *in vitro* by

§Corresponding author.

Raman microspectroscopy. Wang *et al.*[19] were one of the first to experimentally demonstrate that topical application of a glycerol solution with a concentration of 70–80% to the rat skin significantly improved OCT imaging contrast and depth capability. Schulmerich *et al.*[20] first demonstrated Raman spectroscopic diffuse tomographic imaging at OC *in vivo* for canine bone under glycerol treatment. The optical immersion clearing of the cranial bone under action of anhydrous glycerol was studied.[5] Laser Speckle Contrast Imaging (LSCI) demonstrated the effectiveness of aqueous 60% glycerol solution for the investigation of cerebral blood flow in newborn mice without scalp removal and skull thinning.[21] Song *et al.*[22] presented their investigation of glycerol on mouse skin also by confocal microscopy. Dependence of OC effect on glycerol concentration was investigated in Refs. 12 and 23–26. Carneiro *et al.* evaluated free/bound water in tissue using 20–60% glycerol solutions[23] and evaluated the kinetics of the optical properties for colorectal muscle under 40% glycerol action to characterize the dehydration and refractive index matching mechanisms.[26] Genin *et al.*[12] studied the change of optical parameters of rat skin *ex vivo* under the action of aqueous 30%, 50%, 60%, 70%, 85%, and 100% glycerol solutions. The most efficient OC within the spectral range of 500–900 nm was demonstrated by the 60% and 100% solutions. Sufficiently high diffusion rate in combination with high efficiency of OC was demonstrated by the 85% solution of glycerol. According to Ref. 24, the optimal concentration of glycerol to maximize OC was found to be 70%. The efficacy of glycerol was quantitatively evaluated for concentrations from 50 to 90% using OCT by Yoon *et al.*[25] A 70% glycerol solution was determined to be the optimal concentration for the combination method, which utilized both microneedling and sonophoresis to further enhance the transdermal delivery of the OCA.

These researches helped to study of such mechanisms of tissue optical clearing as dehydration, refractive index matching, collagen dissociation and swelling and effects on blood vessels.[6,7,10–12,27–35]

It was found that glycerol caused alteration in the skin morphology due to a dissociation of the collagen fibers.[30,31] The molecular mechanism of glycerol action led to a loss of order in fibril organization that was first investigated by Yeh *et al.*[30] using multiphoton microscopy. The change in collagen organization and size led to a significant reduction in tissue light scattering. Also, it was shown that 75% glycerol solution did not induce any loss of collagen organization.[7] Pure glycerol influence on dorsal mouse skin was investigated by confocal scanning laser microscopy.[36] It was suggested that the glycerol-related clearing effect started when reducing the angular deviation of scattering. Moreover, an increase in anisotropy of scattering with a minor change in the scattering coefficient should be caused by an increase in the size of the scattering particles meaning swelling of collagen fibers in dermis. In Ref. 35, the authors reported that the application of an aqueous 85% glycerol solution to a rat tail tendon fascicle significantly changed not only the scattering properties of the tissue, but also its birefringence and diattenuation. These changes of the collagen structure were irreversible.[30]

Although glycerol is generally nontoxic, long-term treatment with a highly concentrated solution can induce negative tissue effects such as local hemostasis, shrinkage and even tissue necrosis. Topical application or injection of glycerol into skin influenced the state of blood microcirculation in dermis. The OCA diffused to vessel net area, partly penetrated vessel walls, interacted with endothelial and blood cells and led to local osmotic stress and follow up dehydration of tissue and cells.[32] It was found that glycerol caused anhydrous effect on the cutaneous vasculature, but that effect on vessels was reversible with hydration.[33] In addition, transition from oxygenated form of Hb to deoxygenated form for rat skin related to local hemostasis during 84.4% glycerol treatment *in vivo* was investigated.[10] It was found that the topical application high-concentrated glycerol solution on the mesenteric microvessels of a rat *in vivo*[32] and the chick chorioallantoic membrane[34] also led to reduction in blood flow velocity in all microvessels and to stasis with subsequent recovering.

Glycerol diffusion rate in tissues can be a biomarker for differentiation between normal and pathological tissues. It was demonstrated in Refs. 9 and 14 which reported comparative studies of glycerol diffusion in human normal and cancer breast tissues *in vitro* as well as skin and myocardium of rats *ex vivo* in the normal condition and the conditions of alloxan-induced diabetes.

The study of kinetics of tissue OC allowed one to evaluate the glycerol diffusion and permeability coefficients.[12,14] Using these techniques, based on collimated light transmittance measurements for no-fixed *ex vivo* tissue, the diffusion rates of glycerol were determined in myocardium[14] and skin.[12,14]

Thus, a lot of studies using glycerol and different types of tissue generally clarified the main physical and chemical mechanisms of tissue OC: tissue exposure in glycerol solutions causes an effective increase in tissue transparence due to refractive index matching of tissue components and induce dehydration or swelling. Dehydration is caused by osmotic properties of glycerol, and swelling is due to the replacement of water molecules bonded with collagen fibers, by glycerol molecules. However, practical recommendations on optimal glycerol concentrations and duration of action for both *ex vivo* and *in vivo* use are also important. Despite the widespread use of glycerol in the tissue OC, differences in the mechanism of its action at various solution concentrations used are not sufficiently studied. The combined study of glycerol effects on the kinetics of optical, geometrical and weight properties of skin tissues will help in explaining the features of OC using solutions with different glycerol concentrations.

In this paper, we present the results of *ex vivo* measurements of optical, geometrical and weigh changes of rat skin under action of aqueous glycerol solutions in the wide range of concentrations. These data can be helpful for refinement of models developed to evaluate the effective diffusion coefficients of glycerol in tissues.

2. Materials and Methods

We used dehydrated glycerol ("Reachim", Russia) for preparation of aqueous glycerol solutions with volume concentrations of 20%, 30%, 40%, 50%, 60%, 70%, 80%, 90% and 100%. The refractive indices of the solutions were measured by Abbe refractometer (Atago DR-M2/1550, Japan) at the following wavelengths: 450, 480, 486, 546, 589, 644, 656, 680 and 930 nm. The measurements were made at the room temperature ($\sim 20°$C). In this work, we used the following representation of the wavelength, temperature and density dependence of the Lorentz–Lorentz function for aqueous solutions of glycerol:

$$\frac{n^2-1}{n^2+1}\frac{1}{\rho^*} = a_0 + a_1\rho^* + a_2T^* + a_3\lambda^{*2}T^* + \frac{a_4}{\lambda^{*2}} + \frac{a_5}{\lambda^{*2}-\lambda_{\mathrm{UV}}^{*2}} + \frac{a_6}{\lambda^{*2}-\lambda_{\mathrm{IR}}^{*2}} + a_7\rho^{*2},$$

(1)

where n is the refractive index of glycerol solutions, $\rho^* = \rho/\rho_0$ is the relative density of the glycerol solutions, $\rho_0 = 1\,\mathrm{g/mL}$, $\lambda^* = \lambda/\lambda_0$ is the relative wavelength, $\lambda_0 = 589\,\mathrm{nm}$, $\lambda_{\mathrm{UV}} = 229.202\,\mathrm{nm}$, $\lambda_{\mathrm{IR}} = 5432.937\,\mathrm{nm}$, λ is the wavelength (nm), $T^* = T/T_0$ is the relative temperature of the glycerol solutions, and $T_0 = 273.15\,\mathrm{K}$.[37] The density of glycerol solutions ρ were presented in Ref. 38.

The approximation of dispersion dependencies of the measured refractive indices was obtained under the condition that the standard deviation function (SD) is as follows:

$$\mathrm{SD} = \sqrt{\frac{\sum_{i=0}^{N}(n_{\mathrm{calc}i}-n_{\mathrm{exp}i})^2}{N\cdot(N-1)}} < 0.001,$$

where n_{calc} is calculated value and n_{exp} is the measured value of the refractive index, N is the number of points. The coefficients $a_0,\ldots,a_7$ were used to obtain the dispersion dependence of the calculated value of the refractive index.

As the objects of investigation of the kinetics of each of the parameters (optical transmittance, weight, thickness, and area), we used 10 skin samples of laboratory albino outbred rats *ex vivo* (a total of 240 samples; the weight and thickness were measured in the same samples in turn). Before the start of the experiment, the hair was removed using the Veet depilatory cream (Reckitt Benckiser, France). The samples by the size about $10 \times 15\,\mathrm{mm}^2$ were cut using scalpel and scissors. Hypodermal layer was carefully removed from the skin samples.

The collimated transmittance was measured with the spectrometer USB4000-Vis-NIR (Ocean Optics, USA). As a light source halogen lamp HL-2000 (Ocean Optics, USA) was used. Optical fiber cables P400-1-UV-VIS (Ocean Optics, USA) with inner diameter $400\,\mu$m and collimators 74-ACR (Ocean Optics, USA) on its ends were used for delivery of light to the skin sample and collection of the light passed through the sample. To measure the collimated transmittance, the skin samples were fixed on the plastic holder with size $38 \times 17\,\mathrm{mm}^2$ with a

hole with size $8 \times 8 \, \text{mm}^2$ and were placed into the glass cuvette with volume 5 mL between two optical fiber cables.

Kinetics of the collimated transmittance of skin samples in glycerol solutions was registered by the sequential recording of spectra of the collimated transmittance in the range of 500–900 nm every 3–5 min for an hour. Before the measurements, the reference signal from cuvette with glycerol solution and the holder without skin sample was registered. All measurements were carried out at room temperature (about $20°\text{C}$).

The thickness, area and weight of the samples were measured before the experiment and every 5 min after placing them in a Petri dish filled with the test glycerol solution for 60 min. For this, the skin samples were taken out from the Petri dish; the excess of the glycerol was removed from the surface of the sample using a filter paper. Then the weight and the thickness were measured or the samples were photographed to subsequently calculate the sample area.

The weight measurements were performed using electronic balance SA210 (Scientech, USA). The accuracy of the measurements was $\pm 1 \, \text{mg}$.

To measure the thickness, the sample was placed between two glass slides, after which its thickness was measured at five points using a micrometer (Fujisan, China) with an accuracy of $\pm 1 \, \mu\text{m}$. The results were averaged.

Since the skin samples had an imperfect rectangular shape, to accurately determine their area, they were placed on a black test object with a scale and photographed using a digital camera of a smartphone (Fig. 1(a)). The scale bar was used to

determine the conversion factor from linear dimensions in pixels to linear dimensions in millimeters and the size of the entire image. To increase the contrast of the image, it was first processed using the READ _BLUE function of the MathCad software (Parametric Technology Corporation, United States) to extract the blue color component from the full color image. To reduce noise, eliminate glare, etc. a median filter was used. All pixels that were not occupied by the sample were assigned a value of 0 (Fig. 1(b)).

The number of pixels occupied by the sample (with values other than 0) was calculated and converted to square millimeters using the following equation:

$$S = \frac{F(H_S)}{\text{cols}(H_S)\text{rows}(H_S)} \frac{\text{rows}(H)z^2}{\text{cols}(H)}, \qquad (2)$$

where F is a function that calculates the number of pixels occupied by the sample; cols and rows are the number of columns and rows of the image, respectively; H is the original image of the sample, H_S is the image of the sample without background; z is the image width.[39]

The weights, thicknesses and areas were averaged over all samples in the groups with the similar glycerol concentration. The average volumes of the samples were calculated using the averaged values of the thickness and area for each group of the samples.

The temporal dependences of the thickness, area, volume and weight of skin samples obtained in the course of the action of glycerol solutions were normalized to the values measured at the initial moment of time (i.e., before the skin was placed in the solution). Normalized kinetics of the both volume and weight were approximated by a two-exponential equation, the first part describes the kinetics of tissue dehydration (shrinkage), and the second one the kinetics of its swelling:

$$B_{\text{norm}}(t) = \frac{B(t)}{B(t=0)} = A_D \exp\left(-\frac{t}{\tau_w}\right)$$
$$+ B_S\left(1 - \exp\left(-\frac{t}{\tau_g}\right)\right) + y_0, \quad (3)$$

where $B(t)$ and $B(t=0)$ are the values of the measured parameter at time t and $t=0$, respectively; A_D and B_S are the maximum degree of dehydration/shrinkage and swelling of the sample, respectively; τ_w is the characteristic dehydration
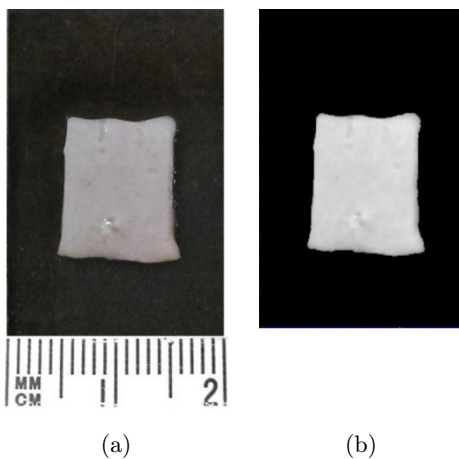

Fig. 1. Typical digital image of a skin sample on a test object with a scale (a) and result of digital image processing (b).

time; τ_g is the characteristic time of tissue swelling; y_0 is the residual value of the magnitude that can be achieved.[39]

3. Results and Discussion

Figure 2 shows spectral dependencies of the refractive index for different glycerol solutions. Table 1 summarizes the approximation coefficients. The refractive index of hydrated collagen fibers from the stroma of bovine eye[40] at the wavelength 589 nm can be considered close to the refractive index of skin dermal hydrated collagen fibers. It is well seen that the refractive indices of 60% glycerol solution and hydrated collagen fibers, which are the main dermal scatterers, have the nearest values (Fig. 2).

In Fig. 3, the typical kinetics of the collimated transmittance of the skin samples in the spectral range of 500–900 nm for an hour is presented. For this figure, the samples with approximately equal initial thickness were taken: 0.48 ± 0.06 mm.
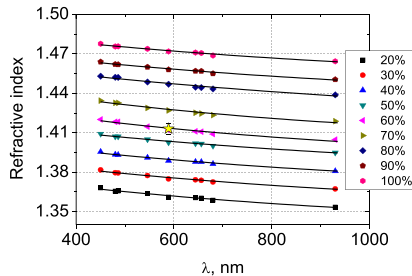
Fig. 2. Spectral dependencies of the refractive index of aqueous glycerol solutions (vol/vol concentrations 20–100%). Symbols show measured data, solid curves correspond the results of approximation. Asterisk corresponds to the refractive index of hydrated collagen fibers from Ref. 40.

Differences in the initial value of T_c are associated with deviations of the initial thickness of the samples.

Matching effect caused by the penetration of glycerol into the interstitial fluid and simultaneous osmotic dehydration of the skin induces an increase in the collimated transmittance of samples. It is well seen that the degree of optical clearing increases with increasing the glycerol concentration, excluding high concentrated solutions (80–100% glycerol solutions induce approximately equal degree of optical clearing). However, kinetics of the optical clearing for solutions used is different. At the glycerol concentration from 20 to 40%, T_c reaches a maximal value and then decreases (Figs. 3(a)–3(c)). With increasing concentration, time of the maximal transparency achievement is shortened, but the degree of T_c value reducing increases. Kinetics of the collimated transmittance is well matched with kinetics of the sample thickness, presented in Fig. 4(a). It is well seen that the decrease in the average thickness of the samples is replaced by an increase when the solutions 20–40% are used. This effect increases with concentration and is maximal for the samples exposure in 40% glycerol solution (about 9%). It can be associated with viscosity of glycerol solution, which increases exponentially with the rise of the concentration. At the concentration 20–40% the dynamical viscosity increases insignificantly (from 1.76 to 3.72 mP·s at the 20°C,[41]), and glycerol penetrates freely to the interstitial fluid of the skin. The characteristic time of dehydration τ_w decreases (Fig. 4(d)) and geometrical and weight parameters of the samples tend to recover after dehydration during an hour (Figs. 4, 5 and Tables 2, 3).

Table 1. Approximation coefficients of the spectral dependencies of the refractive index of the aqueous glycerol solutions.

| Glycerol concentration, vol/vol %	a_0	a_1	a_2	a_3	a_4	a_5	a_6	a_7
20	0.23304	0.02259	-7.44072×10^{-3}	-1.02323×10^{-3}	3.97165×10^{-3}	204.91333	1.15585×10^5	-0.02928
30	0.23347	0.02308	-7.03981×10^{-3}	-9.60732×10^{-4}	3.90605×10^{-3}	180.25039	1.02105×10^5	-0.02874
40	0.23495	0.02449	-5.66769×10^{-3}	-9.28124×10^{-4}	3.76466×10^{-3}	102.57688	5.7761×10^4	-0.03263
50	0.2351	0.02467	-5.52392×10^{-3}	-9.04449×10^{-4}	3.56885×10^{-3}	93.84297	5.32739×10^4	-0.031
60	0.23478	0.02444	-5.82156×10^{-3}	-8.90412×10^{-4}	4.22806×10^{-3}	112.00016	6.48547×10^4	-0.02978
70	0.23461	0.02434	-5.97733×10^{-3}	-8.82573×10^{-4}	4.14344×10^{-3}	118.85235	6.63277×10^4	-0.0274
80	0.23608	0.02559	-4.61197×10^{-3}	-9.48082×10^{-4}	3.42699×10^{-3}	43.46239	2.48359×10^4	-0.02859
90	0.23654	0.02598	-4.18337×10^{-3}	-8.01167×10^{-4}	2.9191×10^{-3}	19.30733	1.08464×10^4	-0.02916
100	0.23634	0.02583	-4.36646×10^{-3}	-7.86929×10^{-4}	2.76153×10^{-3}	29.66142	1.69687×10^4	-0.02703
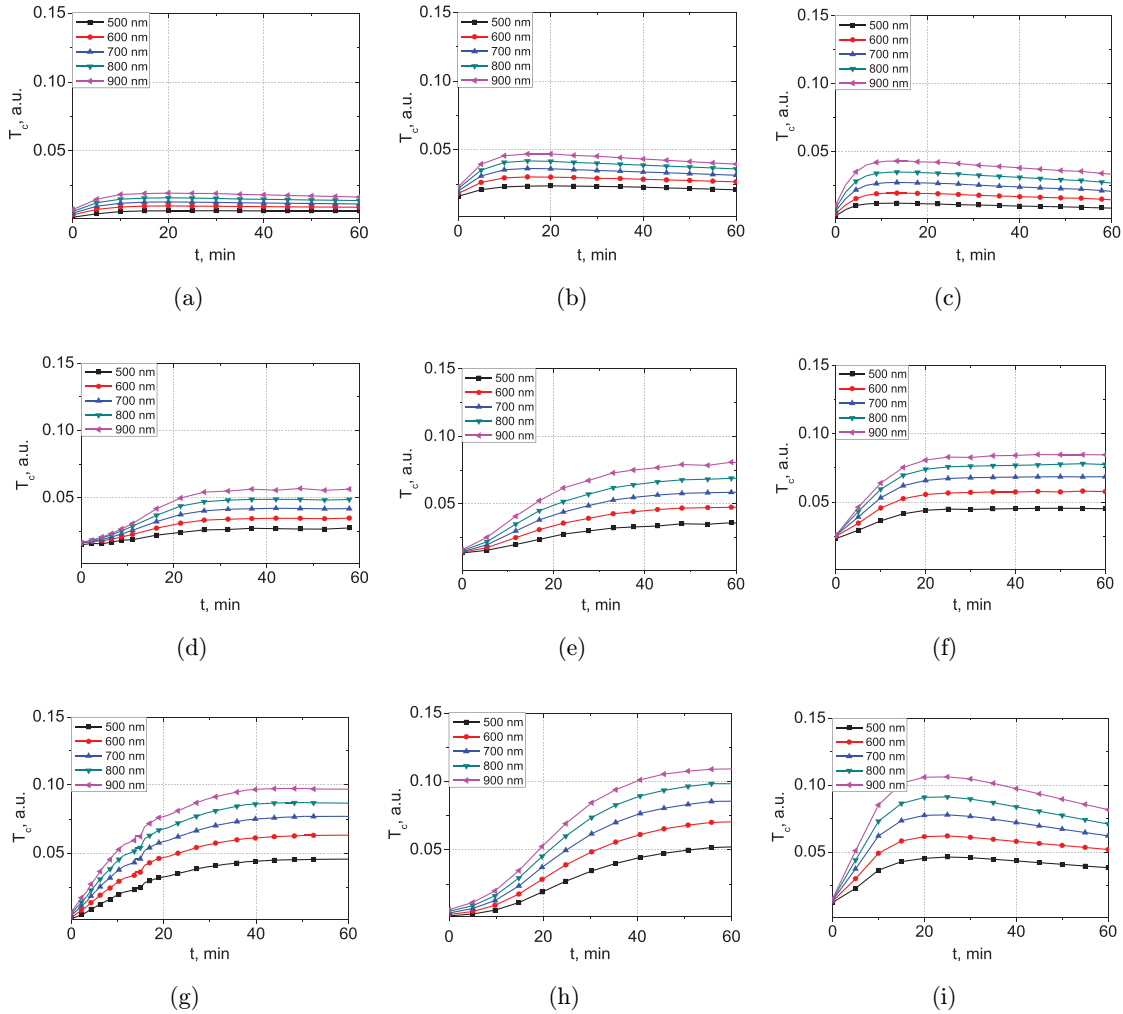
Fig. 3. Typical temporal dependencies of collimated transmittance of rat skin *ex vivo* under action of aqueous glycerol solutions with different (vol/vol) concentrations: (a) 20%, (b) 30%, (c) 40%, (d) 50%, (e) 60%, (f) 70%, (g) 80%, (h) 90% and (i) 100%.

Such recovering can be also caused by hygroscopic properties of glycerol. Glycerol solutions at any concentration gain or supply moisture until a concentration that is in equilibrium with the moisture of the environment is reached. It was shown that each glycerol molecule can bind six water molecules.[42] Thus, glycerol diffusing inside tissue holds water and induces swelling.

Solutions with a concentration of 50% and 60% glycerol are characterized by dynamical viscosity 6.0 and 10.8 mP · s,[40] respectively, and demonstrate transition from exchanging process to predominant dehydration (Fig. 4 and Table 2). Swelling of the sample after exposure in 50% and 60% glycerol is about only 5% and 3%, respectively (Fig. 4(c)); and it is not affecting the kinetics of collimated transmittance (Figs. 3(d) and 3(e)).

The next group of solution with concentrations of 70–90% shows decreasing duration of the dehydration process (Figs. 3(f)–3(h) and 4(d)). Viscosity of the solutions is high (from 22.5 to 219 mP · s[41]); therefore diffusion of glycerol into the skin is hindered, but water diffusion rate increases under action of osmotic pressure. It was shown that at a temperature 300°K, ratio of water diffusion coefficient to glycerol diffusion coefficient in glycerol–water mixtures increases from 2.5 to 5 with an increase in the glycerol mole fraction from 0.14 to 50% (50% corresponds to glycerol weight fraction 0.84).[43] The coefficient of mutual diffusion of glycerol-water mixtures decreases exponentially from 1.025×10^{-9} to $0.014 \times 10^{-9} \, \text{m}^2/\text{s}$ with an increase in the mole fraction of glycerol in mixtures from 0 to 1.[44] Thus, the mobility of water molecules
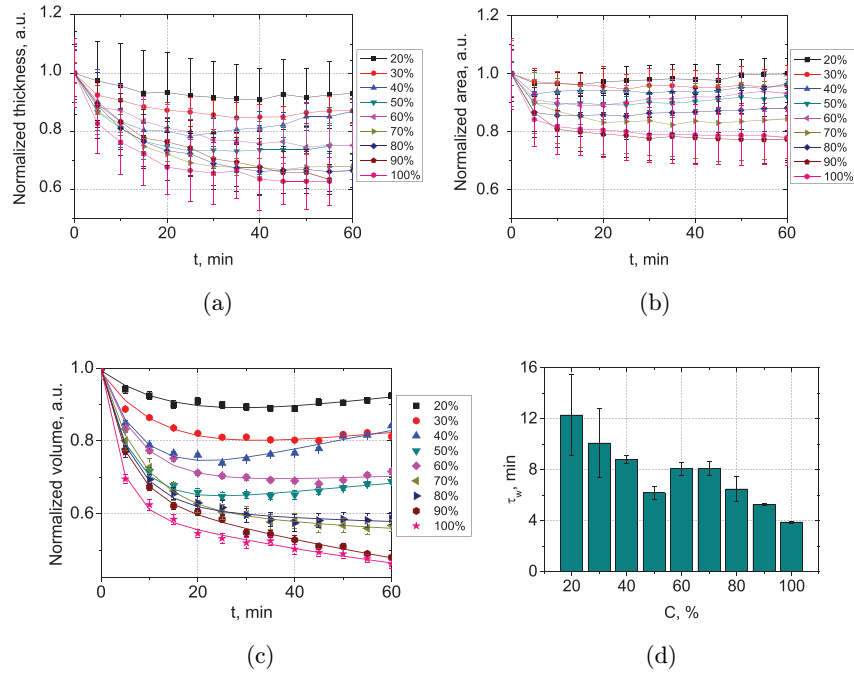
Fig. 4. Normalized averaged kinetics of geometrical parameters of rat skin *ex vivo* under action of aqueous glycerol solutions with vol/vol concentrations from 20% to 100% (a)–(c) and concentration dependence of the sample dehydration characteristic time calculated from the normalized volume approximation dependencies. (d) Parameters were averaged on 10 samples for each concentration.

significantly higher than that of glycerol molecules, therefore dehydration becomes a predominant process during the observation time. We cannot observe the swelling of the tissue (Fig. 4, Table 2). In Table 2, coefficient B_s becomes negative that corresponds to the further dehydration of the samples. The characteristic time of this process τ_s increases with an increase in the concentration of glycerol due to an increase in tissue shrinkage and, consequently, tissue density, as well as the tortuosity of the pathways of water molecules in the tissue.

Separate place has group of the samples immersed in pure glycerol (100%). Glycerol has

colossal dynamical viscosity $(1410\,\text{mP}\cdot\text{s}$[40]$)$; therefore, we consider that it doesn't penetrate practically into the tissue during an hour; and the main cause of the optical clearing is dehydration. However, kinetics of T_c (Fig. 3(i)) demonstrates significant increasing during 10–20 min for different samples and then significant decreasing. At this, the thickness and volume of the samples decrease monotonically down to $39 \pm 8\%$ and $54 \pm 1\%$, respectively, from initial values (Figs. 4(a) and 4(c)). In this case, decreasing collimated transmittance can be induced by increasing volume fraction of the scatterers in the area of detection caused by high

Table 2. Approximated parameters for kinetics of average volumes of rat skin *ex vivo* under action of aqueous glycerol solutions with vol/vol concentrations from 20% to 100%.

C, %	A_D	SD (A_D)	τ_w, min	SD (τ_w)	B_S	SD (B_S)	τ_g, min	SD (τ_g)	y_0	SD (y_0)
20	0.15	0.01	12.3	3.2	0.19	0.07	120.2	19.3	0.85	0.01
30	0.23	0.04	10.1	2.7	0.20	0.10	123.5	9.2	0.76	0.04
40	0.36	0.01	8.8	0.3	0.51	0.02	123.4	0.9	0.63	0.01
50	0.38	0.01	6.2	0.52	0.18	0.01	120.0	8.5	0.61	0.001
60	0.32	0.01	8.1	0.51	0.07	0.02	101.0	10.0	0.64	0.04
70	0.38	0.002	8.1	0.53	−0.13	0.004	96.7	5.8	0.62	0.001
80	0.37	0.01	6.5	0.98	−0.13	0.004	95.0	7.1	0.63	0.01
90	0.34	0.003	5.3	0.06	−0.46	0.05	120.1	19.8	0.66	0.003
100	0.39	0.01	3.9	0.08	−0.39	0.02	132.5	6.4	0.61	0.01

Table 3. Approximated parameters for kinetics of average weights of rat skin *ex vivo* under action of aqueous glycerol solutions with vol/vol concentrations from 20% to 100%.

C, %	A_D	SD (A_D)	τ_w, min	SD (τ_w)	B_S	SD (B_S)	τ_g, min	SD (τ_g)	y_0	SD (y_0)
20	0.09	0.01	11.8	0.4	0.07	0.004	138.1	15.3	0.91	0.001
30	0.13	0.01	9.7	2.4	0.09	0.05	103.8	22.1	0.87	0.01
40	0.26	0.003	5.7	0.51	0.15	0.02	88.3	19.5	0.75	0.004
50	0.30	0.001	6.8	0.61	0.13	0.01	113.7	6.9	0.73	0.001
60	0.11	0.003	4.3	0.2	−0.15	0.01	68.5	6.9	0.89	0.01
70	0.17	0.01	10.6	3.1	−0.08	0.05	108.6	18.3	0.83	0.01
80	0.25	0.004	11.7	1.2	−0.09	0.01	95.3	14.8	0.76	0.04
90	0.15	0.01	6.5	0.8	−0.31	0.02	106.2	20.4	0.84	0.01
100	0.82	0.001	5.8	0.21	−0.07	0.02	160.4	44.6	0.72	0.001

degree of dehydration. Low degree of immersion does not allow compensating for this effect.

Decreasing in the area of the samples is observed for all glycerol concentration just after immersion (Fig. 4(b)) due to the dehydration process. Shrinkage of the samples causes an increase in rigidity and roughness of the tissue. Diffusion of glycerol into the tissue restores its softness and causes smoothing, so the area of the samples increases. In 90% and 100% glycerol solutions, rigidity and roughness of the samples remain for an hour.

Figure 5 and Table 3 show that the kinetics of the skin sample weight is in a good agreement with the other results. A decrease in the weight in the first stage caused by the dehydration and the partial recovery of the parameter is observed only for the samples immersed in the 20–50% glycerol solutions. Starting from the 60% glycerol, dehydration is the predominant process. Concentration dependence of the characteristic dehydration time τ_w, calculated from the normalized volume and weight approximation dependencies are in a good agreement (Figs. 4(b) and 5(b)).

Based on the performed molecular modeling, interaction of the protein molecules with glycerol solutions was studied in Refs. 45 and 46. It was shown that for aqueous solutions with less than 50% glycerol in volume, protein solvation shells have approximately the same composition as the bulk solvent.[45] Thus, a large number of glycerol molecules are in direct contact with the protein. In Ref. 46, the description of the mechanism of collagen fiber swelling was suggested as follows: glycerol molecules pushes out the water bound to collagen. The disruption of hydrogen bonds net occurs because glycerol molecules bound to collagen by alcohol groups, "stick out" their hydrophobic parts (CH_2-groups), and prevent formation of new hydrogen bonds. It leads to fibril protein swelling.[35,46] It was also shown that the increase in relative volume in collagen peptide is maximal when 40% glycerol is used;[46] efficacy of the optical clearing[12] and the light penetration depth measured by OCT[47] were maximal when 60% and 70% glycerol solutions were used, respectively. These data are in a good agreement with our results. The replacement of the
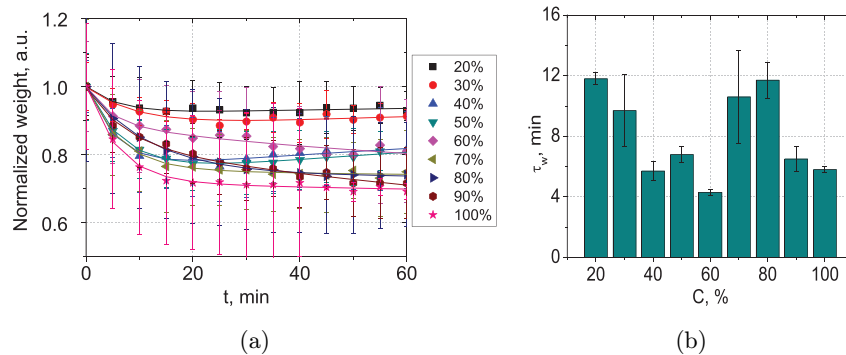

Fig. 5. Normalized averaged kinetics of weigh of rat skin *ex vivo* under action of aqueous glycerol solutions with vol/vol concentrations from 20% to 100% (a) and concentration dependence of the sample dehydration characteristic time calculated from the normalized weight approximation dependencies (b). Weight was averaged on 10 samples for each concentration.

7. X. Wen, Z. Mao, Z. Han, V. V. Tuchin, D. Zhu, "*In vivo* skin optical clearing by glycerol solutions: Mechanism," *J. Biophoton.* **3**, 44–52 (2010).

8. H. Zhong, Z. Guo, H. Wei, C. Zeng, H. Xiong, Y. He, S. Liu, "*In vitro* study of ultrasound and different-concentration glycerol-induced changes in human skin optical attenuation assessed with optical coherence tomography," *J. Biomed. Opt.* **15**, 036012 (2010).

9. H. Q. Zhong, Z. Y. Guo, H. J. Wei, C. C. Zeng, H. L. Xiong, Y. H. He, S. H. Liu, "Quantification of glycerol diffusion in human normal and cancer breast tissues in vitro with optical coherence tomography," *Laser Phys. Lett.* **7**, 315–320 (2010).

10. E. A. Genina, A. N. Bashkatov, Yu. P. Sinichkin, V. V. Tuchin, "Optical clearing of skin under action of glycerol: *Ex vivo* and *in vivo* investigations," *Opt. Spectrosc.* **109**, 225–231 (2010).

11. T. Yu, X. Wen, V. V. Tuchin, Q. Luo, D. Zhu, "Quantitative analysis of dehydration in porcine skin for assessing mechanism of optical clearing," *J. Biomed. Opt.* **16**, 095002 (2011).

12. V. D. Genin, D. K. Tuchina, A. J. Sadeq, E. A. Genina, V. V. Tuchin, A. N. Bashkatov, "*Ex vivo* investigation of glycerol diffusion in skin tissue," *J. Biomed. Photon. Eng.* **2**, 010303 (2016).

13. T. Yu, Y. Qi, J. Wang, W. Feng, J. Xu, J. Zhu, Y. Yao, H. Gong, Q. Luo, D. Zhu, "Rapid and prodium iodide-compatible optical clearing method for brain tissue based on sugar/sugar-alcohol," *J. Biomed. Opt.* **21**, 081203 (2016).

14. D. K. Tuchina, A. N. Bashkatov, A. B. Bucharskaya, E. A. Genina, V. V. Tuchin, "Study of glycerol diffusion in skin and myocardium *ex vivo* under the conditions of developing alloxan-induced diabetes," *J. Biomed. Photon. Eng.* **3**, 020302 (2017).

15. E. A. Genina, A. N. Bashkatov, Yu. P. Sinichkin, I. Yu. Yanina, V. V. Tuchin, "Optical clearing of biological tissues: Prospects of application in medical diagnostics and phototherapy," *J. Biomed. Photon. Eng.* **1**, 22–58 (2015).

16. A. Yu. Sdobnov, M. E. Darvin, E. A. Genina, A. N. Bashkatov, J. Lademann, V. V. Tuchin, "Recent progress in tissue optical clearing for spectroscopic application," *Spectrochim. Acta A: Mol. Biomol. Spectrosc.* **197**, 216–229 (2018).

17. R. Cicchi, F. S. Pavone, D. Massi, D. D. Sampson, "Contrast and depth enhancement in two-photon microscopy of human skin *ex vivo* by use of optical clearing agents," *Opt. Exp.* **13**, 2337–2344 (2005).

18. D. Huang, W. Zhang, H. Zhong, H. Xiong, X. Guo, Z. Guo, "Optical clearing of porcine skin tissue in vitro studied by Raman microspectroscopy," *J. Biomed. Opt.* **17**, 015004 (2012).

19. R. K. Wang, X. Xu, V. V. Tuchin, J. B. Elder, "Concurrent enhancement of imaging depth and contrast for optical coherence tomography by hyperosmotic agents," *JOSA B* **18**, 948–953 (2001).

20. M. V. Schulmerich, K. A. Dooley, T. M. Vanasse, S. A. Goldstein, M. D. Morris, "Subsurface and transcutaneous Raman spectroscopy and mapping using concentric illumination rings and collection with a circular fiber optic array," *Appl. Spectrosc.* **61**, 671–678 (2007).

21. P. A. Timoshina, E. M. Zinchenko, D. K. Tuchina, M. M. Sagatova, O. V. Semyachkina-Glushkovskaya, V. Valery, "Laser speckle contrast imaging of cerebral blood flow of newborn mice at optical clearing," *Proc. SPIE* **10336**, 1033610 (2017).

22. E. Song, Y. Ahn, J. Ahn, S. Ahn, C. Kim, S. Choi, R. M. Boutilier, Y. Lee, P. Kim, H. Lee, "Optical clearing assisted confocal microscopy of *ex vivo* transgenic mouse skin," *Opt. Laser Technol.* **73**, 63–76 (2015).

23. I. Carneiro, S. Carvalho, R. Henrique, R. Oliveira, V. V. Tuchin, "Simple multimodal optical technique for evaluation of free/bound water and dispersion of human liver tissue," *J. Biomed. Opt.* **22**, 125002 (2017).

24. T. Son, B. Jung, "Cross-evaluation of optimal glycerol concentration to enhance optical clearing efficacy," *Skin Res. Technol.* **21**, 327–332 (2015).

25. J. Yoon, D. Park, T. Son, J. Seo, J. S. Nelson, B. Jung, "A physical method to enhance transdermal delivery of a tissue optical clearing agent: Combination of microneedling and sonophoresis," *Lasers Surg. Med.* **42**, 412–417 (2010).

26. I. Carneiro, S. Carvalho, R. Henrique, R. Oliveira, V. V. Tuchin, "Kinetics of optical properties of colorectal muscle during optical clearing," *IEEE J. Sel. Top. Quantum. Electron.* **25**, 7200608 (2019).

27. E. A. Genina, A. N. Bashkatov, A. A. Korobko, E. A. Zubkova, V. V. Tuchin, I. Yaroslavsky, G. B. Altshuler, "Optical clearing of human skin: Comparative study of permeability and dehydration of intact and photothermally perforated skin," *J. Biomed. Opt.* **13**, 021102 (2008).

28. V. Hovhannisyan, P.-S. Hu, S.-J. Chen, C.-S. Kim, C.-Y. Dong, "Elucidation of the mechanisms of optical clearing in collagen tissue with multiphoton imaging," *J. Biomed. Opt.* **18**, 046004 (2013).

29. Z. Mao, D. Zhu, Y. Hu, X. Wen, Z. Han, "Influence of alcohols on the optical clearing effect of skin *in vitro*," *J. Biomed. Opt.* **13**, 021104 (2008).

30. A. T. Yeh, B. Choi, J. S. Nelson, B. J. Tromberg, "Reversible dissociation of collagen in tissues," *J. Invest. Dermatol.* **121**, 1332–1335 (2003).

31. J. M. Hirshburg, K. M. Ravikumar, W. Hwang, A. T. Yeh, "Molecular basis for optical clearing of

collagenous tissues," *J. Biomed. Opt.* **15**, 055002 (2010).

32. E. I. Galanzha, V. V. Tuchin, A. V. Solovieva, T. V. Stepanova, Q. Luo, H. Cheng, "Skin backreflectance and microvascular system functioning at the action of osmotic agents," *J. Phys. D: Appl. Phys.* **36**, 1739–1746 (2003).

33. G. Vargas, A. Readinger, S. S. Dosier, A. J. Welch, "Morphological changes in blood vessels produced by hyperosmotic agents and measured by optical coherence tomography," *Photochem. Photobiol.* **77**, 541–549 (2003).

34. D. Zhu, J. Zhang, H. Cui, Z. Mao, P. Li, Q. Luo, "Short-term and long-term effects of optical clearing agents on blood vessels in chick chorioallantoic membrane," *J. Biomed. Opt.* **13**, 021106 (2008).

35. A. N. Bashkatov, K. V. Berezin, K. N. Dvoretskiy, M. L. Chernavina, E. A. Genina, V. D. Genin, V. I. Kochubey, E. N. Lazareva, A. B. Pravdin, M. E. Shvachkina, P. A. Timoshina, D. K. Tuchina, D. D. Yakovlev, D. A. Yakovlev, I. Yu. Yanina, O. S. Zhernovaya, V. V. Tuchin, "Measurement of tissue optical properties in the context of tissue optical clearing," *J. Biomed. Opt.* **23**, 091416 (2018).

36. R. Samatham, K. G. Phillips, S. L. Jacques, "Assessment of optical clearing agents using reflectance-mode confocal scanning laser microscopy," *J. Innov. Opt. Health Sci.* **3**, 183–188 (2010).

37. P. Schiebener, J. Straub, J. M. H. LeveltSengers, J. S. Gallagher, "Refractive index of water and steam as function of wavelength, temperature and density," *J. Phys. Chem. Ref. Data* **19**, 677–717 (1990).

38. M. V. Noble, A. B. Garrett, "A thermodynamic study of lead chloride in dioxane-water by means of electromotive force and solubility data at 25°; the acetone-, ethanol-, dioxane-, glycerol–water–lead chloride systems," *J. Am. Chem. Soc.* **66**, 231–235 (1944).

39. D. K. Tuchina, A. N. Bashkatov, E. A. Genina, V. V. Tuchin, "Investigation of the impact of immersion agents on weight and geometric parameters of myocardial tissue *in vitro*," *Biophysics* **63**, 791–797 (2018).

40. V. V. Tuchin, *Tissue Optics: Light Scattering Methods and Instruments for Medical Diagnosis*, SPIE Tutorial Text in Optical Engineering, 3rd Edition, SPIE Press, Washington, Bellingham (2015).

41. M. L. Sheeley, "Glycerol viscosity tables," *Ind. Eng. Chem.* **24**, 1060–1064 (1932).

42. J. W. Wiechers, J. C. Dederen, A. V. Rawlings, "Moisturization mechanisms: Internal occlusion by orthorhombic lipid phase stabilizers — a novel mechanism of skin moisturization," *Skin Moisturization*, Chap. 19, A. V. Rawlings, J. J. Leyden, Eds., pp. 309–321, Taylor and Francis, London (2009).

43. F. O. Akinkunmi, D. A. Jahn, N. Giovambattista, "Effects of temperature on the thermodynamic and dynamical properties of glycerol-water mixtures: A computer simulation study of three different force fields," *J. Phys. Chem. B* **119**, 6250–6261 (2015).

44. G. D'Errico, O. Ortona, F. Capuano, V. Vitagliano, "Diffusion coefficients for the binary system glycerol + water at 25°C. A velocity correlation study," *J. Chem. Eng. Data* **49**, 1665–1670 (2004).

45. N. Chéron, M. Naepels, E. Pluhařová, D. Laage, "Protein preferential solvation in water: Glycerol mixtures," *J. Phys. Chem. B* **124**, 1424–1437 (2020).

46. K. V. Berezin, K. N. Dvoretskiy, M. L. Chernavina, A. M. Likhter, V. V. Smirnov, I. T. Shagautdinova, E. M. Antonova, E. Yu. Stepanovich, E. A. Dzhalmuhambetova, V. V. Tuchin, "Molecular modeling of immersion optical clearing of biological tissues," *J. Mol. Model.* **24**, 45 (2018).

47. E. Youn, T. Son, H.-S. Kim, B. Jung, "Determination of optimal glycerol concentration for optical tissue clearing," *Proc. SPIE* **8207**, 82070J (2012).

48. R. K. Wang, J. B. Elder, "Propylene glycol as a contrasting agent for optical coherence tomography to image gastrointestinal tissues," *Lasers Surg. Med.* **30**, 201–208 (2002).

49. X. Xu, Q. Zhu, "Sonophoretic delivery for contrast and depth improvement in skin optical coherence tomography," *IEEE J. Sel. Top. Quant. Electron.* **14**, 56–61 (2008).

50. J. Wang, Y. Liang, S. Zhang, Y. Zhou, H. Ni, Y. Li, "Evaluation of optical clearing with the combined liquid paraffin and glycerol mixture," *Biomed. Opt. Exp.* **2**, 2329–2338 (2011).

51. S. V. Zaitsev, Y. I. Svenskaya, E. V. Lengert, G. S. Terentyuk, A. N. Bashkatov, V. V. Tuchin, E. A. Genina, "Optimized skin optical clearing for optical coherence tomography monitoring of encapsulated drug delivery through the hair follicles," *J. Biophoton.* **13**, e201960020 (2020).

52. S. Tran, S. Zaytsev, V. Charykova, M. Yusupova, A. Bashkatov, E. Genina, V. Tuchin, W. Blondel, M. Amouroux, "Analysis of image features for the characterization of skin optical clearing kinetics performed on *in vivo* and *ex vivo* human skin using Linefield-Confocal Optical Coherence Tomography (LC-OCT)," *Proc. SPIE* **11553**, 115532P (2020).